Emulation of Energy Storage Flywheels on a Rotor-AMB Test Rig

Xujun Lyu[a,b], Long Di[b], Se Young Yoon[b], Zongli Lin[b], Yefa Hu[a]

[a] School of Mechanical and Electronic Engineering, Wuhan University of Technology, Wuhan, Hubei, China, emmalxj198762@gmail.com, huyefa@whut.edu.cn

[b] Charles L. Brown Department of Electrical and Computer Engineering, and Rotating Machinery and Controls Laboratory (ROMAC), University of Virginia, Charlottesville, VA 22904-4743, USA, {ld4vv, syy5b, zl5y}@virginia.edu

***Abstract*—Because of their many appealing features, such as high specific energy, high specific power, ultra-compactness, short charging time (in minutes), long life span and no pollution, energy storage flywheels suspended on active magnetic bearings (AMBs) have drawn worldwide attention. In this paper, we use an existing rotor-AMB test rig to emulate the operation of energy storage flywheels suspended on AMBs. The test rig contains four active magnetic bearings, two located at the two ends of the rotor, one located at the rotor mid-span and the last located at the rotor quarter span. We will use the two magnetic bearings in the mid and quarter spans to emulate the negative stiffness of the generator and the gyroscopic effect of the flywheel disk. Simulation and experimental results are presented.**

I. Introduction

With the constant development of the economy and the society, the demand for energy storage, which helps to maintain the power system stability, improve the power quality and aid distributed generation, keeps rising [1]. Compared with other energy storage technologies such as super conducting magnetic energy storage, conventional electrochemical batteries and ultra capacitors, flywheels have notable advantages such as high specific energy, high specific power, ultra-compactness, short charging time (in minutes), long life span and no pollution. These benefits of flywheels make them ideal for storing energy in space applications such as satellites, spacecraft and space stations [2]. For hybrid electric vehicles, flywheels can discharge rapidly in order to improve the drivability of vehicles under acceleration or hill-climbing condition. On the other hand, when under deceleration or down-hill condition, flywheels charge quickly in order to improve the efficiency in storing the regenerative energy [3]–[5]. Flywheels are also used for regulating the peak power load of grids, wind power systems and uninterruptible power systems.

Flywheel energy storage systems are typical mechanical batteries. The kinetic energy is stored in a high speed rotating disk of the flywheel ([3], [6]). This mechanical energy is converted back to electric energy by a generator, which is mounted on the same rotor as the flywheel disk. The stored energy for a flywheel system is proportional to the square of the rotating speed Ω, and is given by

$$E = \frac{1}{2} J_{\mathrm{p}} \Omega^2, \tag{1}$$

where J_{p} is the polar moment of inertia of the flywheel disk.

Advanced flywheels operate at high rotating speeds to store a large amount of energy, which results in a high demand on the bearing system for stability and performance. The conventional rolling element bearings, sliding bearings and hydraulic bearings are not adequate to meet such a demand. Active magnetic bearings use magnetic forces to suspend the rotor, and the forces they produce can be actively controlled. Moreover, they possess appealing features such as no mechanical contact, no friction losses, no wear, high speed capability and clean operation. As a result, active magnetic bearings are ideal for supporting high-speed flywheel rotors.

Compared with rotors in many other applications, rotors in the flywheel systems are highly complex. First, in an effort to minimize the overall size of the system, the flywheel disk and the generator are usually mounted on the same shaft, causing a coupling effect between the generator and the rotor dynamics [3]. Second, unlike with applications where the ratio of polar-to-transverse moments of inertia is small and the gyroscopic effects can be neglected ([7], [9]), the large flywheel disks generate strong gyroscopic effects that have to be taken into account in the design of the AMB controller.

The complexities of the flywheel systems entail sophisticated AMB controllers. Brown et al. [7] and Dever et al. [8] confirmed that gyroscopic modes can be stabilized by using cross-axis proportional gains and experimentally demonstrated this fact on the NASA Glenn D1 flywheel. Ahrens et al. [9] and Kucera et al. [10] proposed a cross feedback control method to compensate gyroscopic effects of flywheel AMB systems and experimental results showed that it improve system performance. Hawkins et al. [11] used a gain-scheduled MIMO control algorithm to control an energy storage flywheel, with the consideration of gyroscopic effects. Sivrioglu et al. [12] used a nonlinear control approach with an H_∞ compensator for a zero-bias flywheel AMB system, and experimental results showed that it is a reliable method to control the rotor. Sakai et al. [13] designed a new passivity based control without conventional cross-feedback, and both the simulation and experimental results on a flywheel AMB system showed its advantages in terms of low computational costs and strong robustness.

In summary, the control of flywheel AMB systems has been studied extensively in the literature. Despite this abundance of resources in the literature, the experimental validation of

the theoretical results presented in many of these papers has always been a difficult task. The reason is that it is very expensive and technically challenging to build a flywheel AMB test rig. Among many difficulties, specialized material and complex manufacturing techniques are required to withstand the stress of high speed rotation. We propose to emulate the rotordynamic characteristics of energy storage flywheels on an existing rotor AMB test rig in the Rotating Machinery and Controls Laboratory (ROMAC) at University of Virginia. The test rig contains four active magnetic bearings, two located at the two ends of the rotor, one at the mid span and the other at the quarter span.

The remainder of this paper is organized as follows. Section II describes the rotor AMB test rig and state the problem to be solved in this paper. Section III analyzes the negative stiffness caused by the generator and the gyroscopic effects of the flywheel disk. Section IV presents both the simulation and experimental results. Section V draws the conclusions to this paper.

II. The Test Rig and Problem Statement

Shown in Fig. 1 is a schematic drawing of the rotor-AMB test rig [14] we are to use to emulate the operation of an energy storage flywheel system. This rotor-AMB test rig is a research platform constructed in our ROMAC laboratory. The original purpose of this test rig was to emulate an industrial size centrifugal gas compressor [15]. In particular, disk 1 and disk 2 emulate the wheels in a compressor. There are four AMBs in the test rig. Two radial support AMBs are located at the two ends of the rotor. One exciter AMB is at the mid-span and the other is at the quarter span of the rotor. This combination of four radial AMBs allows the simulation of different operating conditions of the compressor.

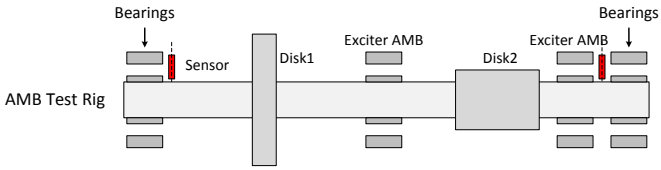

Figure 1: A schematic of the rotor-AMB test rig at University of Virginia.

The rotor in the test rig is 1.23 m long and weights 44.9 kg. Four laminated steel journals are mounted on the shaft respectively for the two radial support AMBs at the non-driven end (NDE) and driven end (DE), and the two radial exciter AMBs at the rotor mid and quarter spans. There are also two auxiliary ball bearings mounted at the support AMB locations to prevent damage to the AMBs in the event of a rotor drop. A 3.7 kW high speed motor with variable frequency drive (VFD), Colombo RS-90/2, drives the rotor in the test rig to speeds up to 18,000 rpm. The entire flexible rotor AMB test rig is shown in Fig. 2.

We use the two AMBs in the mid and quarter spans to emulate the negative stiffness of the generator and the gyroscopic effects of the flywheel disk on the rotor dynamics.

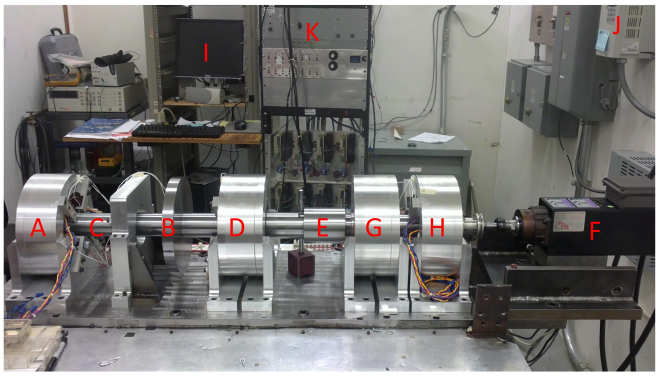

A: Non-driven End Support AMB
B: Gyroscopic Disk 1
C: Rotor Shaft
D: Mid-span Disturbance AMB
E: Gyroscopic Disk 2
F: Electric Motor
G: Quarter-span Disturbance AMB
H: Driven End Support AMB
I: Control Station
J: Variable Frequency Drive
K: Amplifiers & Sensor Conditioning Station

Figure 2: An overview of the flexible rotor AMB test rig.

III. Analysis of Flywheels

The generator mounted on the rotor and the gyroscopic effects caused by the flywheel disk both affect the rotor dynamics of the AMB system. The motion equation of the AMB system is given by

$$M\ddot{q} + (C + \Omega G)\dot{q} + Kq = F_{\text{mag}} + F_{\text{ext}}, \tag{2}$$

where,

M: the symmetric rotor mass matrix,
C: the symmetric support damping matrix,
G: the skew-symmetric gyroscopic effect matrix,
K: the symmetric support stiffness matrix,
Ω: the rotating speed,
F_{mag}: the forces provided by support AMBs,
F_{ext}: the external forces acting on the rotor,
q: the generalized displacement vector.

In the following subsections, we will analyze the effects of the generator and the flywheel disk on the rotor dynamics.

A. Negative Stiffness Caused by the Generator

The effect of the generator on the rotor dynamics is in the form of radial forces, which can be represented as a negative stiffness. Kascak et al. [16] calculated the forces on the rotor caused by a generator for different rotor displacements from the center. It was shown that for small displacements the negative stiffness is about 9.76×10^4 N/m. We use the exciter AMB at the quarter span to emulate this negative stiffness effect of the generator.

B. Gyroscopic Effects of the Flywheel Disk

The rotor subjected to gyroscopic effects will tilt when rotating [17]. A change in the direction of the rotational axis in a spinning flywheel results in a precession rotation generated by the gyroscopic effect. Consider a rotary disk in Fig. 3 mounted on a rigid and massless shaft, spinning about the z axis with an angular velocity Ω rad/s. A precession of the rotor on the x-z plane generates a gyroscopic moment $M_{x\text{G}}$ about

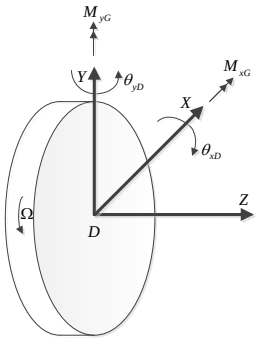

Figure 3: A schematic of gyroscopic effect of the flywheel disk.

the x-axis, which in turn rotates the orientation of the z axis on the y-z plane. Similarly, $M_{y\mathrm{G}}$ represents the gyroscopic moment generated by a precession on the y-z plane.

For the disk, the gyroscopic moments are given by,

$$M_{x\mathrm{G}} = J_{\mathrm{p}}\Omega\dot{\theta}_{y\mathrm{D}}, \tag{3}$$

$$M_{y\mathrm{G}} = -J_{\mathrm{p}}\Omega\dot{\theta}_{x\mathrm{D}}, \tag{4}$$

where $\theta_{x\mathrm{D}}$ and $\theta_{y\mathrm{D}}$ are the mass center angular displacements in the x and y directions, respectively. J_{p} is the polar moment of inertia of the disk.

Fig. 3 illustrates the angular displacement of the disk about its mass center. Because the disk can now rotate simultaneously about x and y axes, the rate of change of angular momentum due to the angular acceleration about these axes also needs to be added to the contribution from the disk polar moment of inertia [18]. Hence, the internal moments of the disk about the x-axis, $M_{x\mathrm{D}}$, and about the y-axis, $M_{y\mathrm{D}}$, are given respectively by

$$M_{x\mathrm{D}} = J_{\mathrm{t}}\ddot{\theta}_{x\mathrm{D}} + J_{\mathrm{p}}\Omega\dot{\theta}_{y\mathrm{D}}, \tag{5}$$

$$M_{y\mathrm{D}} = J_{\mathrm{t}}\ddot{\theta}_{y\mathrm{D}} - J_{\mathrm{p}}\Omega\dot{\theta}_{x\mathrm{D}}, \tag{6}$$

where J_{t} is the transverse moment of inertia of the disk; $J_{\mathrm{t}}\ddot{\theta}_{x\mathrm{D}}$ and $J_{\mathrm{t}}\ddot{\theta}_{y\mathrm{D}}$ are respectively the inertia about the x and y axes.

For the rotor-AMB test rig shown in Fig. 2, we use the two exciter AMBs at the rotor mid and quarter spans to emulate the gyroscopic moments exerted by the flywheel disk located between the exciter bearings, as shown in Fig. 4. In the figure, F_{x1} and F_{x2} are the external forces generated by the exciter bearings in the x axis. In order to emulate the gyroscopic effect caused by the precession about the x axis, moment which equal to $-M_{y\mathrm{D}}$ are generated based on F_{x1} and F_{x2}, and it is essentially equivalent to the rotor internal moment around x axis. Similarly, F_{y1} and F_{y2} are the exciter bearing forces emulating the gyroscopic effect caused by a precession about the y axis. We use the exciter AMBs at the rotor mid span to generate the forces F_{x1} and F_{y1} and the exciter AMBs at the rotor quarter span to generate the forces F_{x2} and F_{y2}. The relationships between the gyroscopic moments and corresponding exciter AMB forces are as follows,

$$-M_{x\mathrm{D}} = aF_{y1} - bF_{y2}, \tag{7}$$

$$-M_{y\mathrm{D}} = -aF_{x1} + bF_{x2}, \tag{8}$$

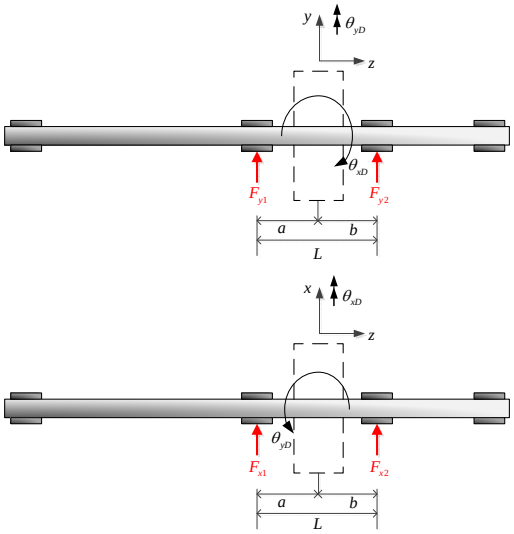

Figure 4: A diagram for the emulation of gyroscopic effects.

$$-F_{x1} = F_{x2}, \tag{9}$$

$$-F_{y1} = F_{y2}, \tag{10}$$

where a and b are the distances between the center of the flywheel disk we want to emulate and the exciter AMBs at the rotor mid and quarter spans, respectively.

For AMBs, the magnetic forces are given by,

$$F_{x1} = K_{\mathrm{i}1}i_{\mathrm{p}x1} - K_{x1}x_1, \tag{11}$$

$$F_{x2} = K_{\mathrm{i}2}i_{\mathrm{p}x2} - K_{x2}x_2, \tag{12}$$

$$F_{y1} = K_{\mathrm{i}1}i_{\mathrm{p}y1} - K_{x1}y_1, \tag{13}$$

$$F_{y2} = K_{\mathrm{i}2}i_{\mathrm{p}y2} - K_{x2}y_2, \tag{14}$$

where,

$K_{\mathrm{i}1}$: current gain of the mid-span AMB,
$K_{\mathrm{i}2}$: current gain of the quarter-span AMB,
K_{x1}: negative stiffness of the mid-span AMB,
K_{x2}: negative stiffness of the quarter-span AMB,
x_1: rotor x axis displacement at the mid span,
x_2: rotor x axis displacement at the quarter span,
y_1: rotor y axis displacement at the mid span,
y_2: rotor y axis displacement at the quarter span,
$i_{\mathrm{p}x1}$: current for the mid-span AMB to generate F_{x1},
$i_{\mathrm{p}x2}$: current for the quarter-span AMB to generate F_{x2},
$i_{\mathrm{p}y1}$: current for the mid-span AMB to generate F_{y1},
$i_{\mathrm{p}y2}$: current for the quarter-span AMB to generate F_{y2}.

The displacements x_1, y_1, x_2 and y_2 are approximated by the angular displacements $\theta_{x\mathrm{D}}$ and $\theta_{y\mathrm{D}}$ by the following equations,

$$\theta_{x\mathrm{D}} \approx \frac{y_2 - y_1}{L}, \tag{15}$$

$$\theta_{y\mathrm{D}} \approx \frac{x_2 - x_1}{L}. \tag{16}$$

In order to emulate the gyroscopic couple using the exciter bearings, we need to find the expressions of the currents. Substituting (11)-(16) into (5)-(10) results in,

$$i_{\mathrm{p}x1} = \frac{K_{x1}}{K_{\mathrm{i}1}}x_1 + \frac{J_{\mathrm{t}}}{K_{\mathrm{i}1}L^2}(\ddot{x}_2 - \ddot{x}_1) - \frac{J_{\mathrm{p}}\Omega}{K_{\mathrm{i}1}L^2}(\dot{y}_2 - \dot{y}_1), \tag{17}$$

$$i_{px2} = \frac{K_{x2}}{K_{i2}} x_2 - \frac{J_t}{K_{i2} L^2}(\ddot{x}_2 - \ddot{x}_1) + \frac{J_p \Omega}{K_{i2} L^2}(\dot{y}_2 - \dot{y}_1), \quad (18)$$

$$i_{py1} = \frac{K_{x1}}{K_{i1}} y_1 - \frac{J_t}{K_{i1} L^2}(\ddot{y}_2 - \ddot{y}_1) - \frac{J_p \Omega}{K_{i1} L^2}(\dot{x}_2 - \dot{x}_1), \quad (19)$$

$$i_{py2} = \frac{K_{x2}}{K_{i2}} y_2 + \frac{J_t}{K_{i2} L^2}(\ddot{y}_2 - \ddot{y}_1) + \frac{J_p \Omega}{K_{i2} L^2}(\dot{x}_2 - \dot{x}_1). \quad (20)$$

We can then carry out the simulation of the gyroscopic effects with the forces generated by the exciter AMBs to make it equal to the gyroscopic forces generated by the flywheel disk.

IV. Simulation and Experimental Results

In order to verify the method presented in Section III, a simulation study is first conducted based on the Simulink model derived from the experimental test rig, which contains all essential components of the rotor-AMB system. The Simulink model is formulated in a state space form consisting of 36 states with 12 inputs and 20 outputs. The 12 inputs include the unbalance forces, external forces from the exciter AMBs and the control voltages for the support AMBs; the 20 outputs include the rotor displacements at the four AMB locations, the corresponding displacement sensor outputs, and the support AMB forces.

Because of the complex dynamics and the uncertainties in the test rig, the AMB system is stabilized by a model based μ-synthesis controller [14], which is formulated in a state space form with 48 states, 4 inputs and 4 outputs. The controller can effectively handle the first and second flexible modes at near 243 Hz and 552 Hz, respectively.

For the flywheel disk, the polar moment of inertia is $J_p = 0.21\,\text{kg}\cdot\text{m}^2$ and the transverse moment of inertia is $J_t = 0.105\,\text{kg}\cdot\text{m}^2$. The properties of the exciter AMBs are summarized in Table I. The effect on the test rig model caused by the added negative stiffness and the emulated gyroscopic forces are shown and discussed in the following subsections.

Table I: Exciter AMBs Properties

Property	mid/quarter	Units
Bias current, I_b	1	A
Number of poles, n	8	--
Estimated air gap flux density, B	0.27	T
Current gain, K_i	94/91	N/A
Negative stiffness, K_x	165/186	kN/m
Copper turns, N	94	--
Projected pole area, A_p	700	mm^2
Nominal air gap, g_0	0.575/0.491	mm

A. Simulation of Generator Effects

The generator effect is in the form of radial forces, and it is interpreted as a negative stiffness acting on the rotor. The exciter AMB at the quarter span is used to provide the required negative stiffness around 9.76×10^4 N/m. Shown in Figs. 5 and 6 are the rotor displacements without and with the generator negative stiffness at the speed of 6,000 rpm, respectively. We observe that the peak rotor displacement at the quarter-span bearing under the μ-synthesis control is less than 2×10^{-5} m (0.78 mils) for both cases, which corresponds to a peak force from the generator negative stiffness of about 1 N. It is observed that the disturbance force is small and its effect on the rotor dynamics is minimal for even higher rotating speeds up to 15,000 rpm.

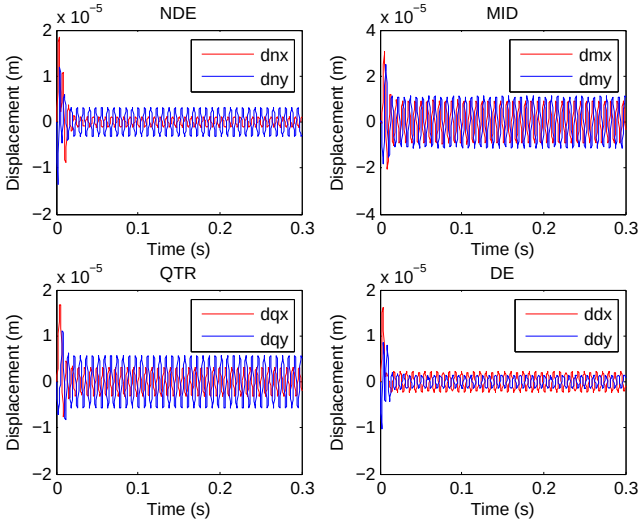

Figure 5: Rotor displacements without the generator negative stiffness.

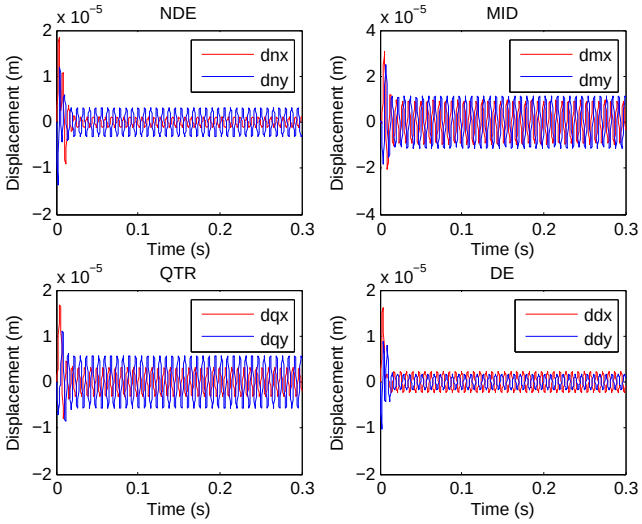

Figure 6: Rotor displacements with the generator negative stiffness.

B. Simulation of Gyroscopic Effects

The gyroscopic effect is emulated using both the mid-span and quarter-span AMBs. The perturbation currents are generated following Eqs. (17)-(20). In order to verify that the emulated gyroscopic effect is generated properly, the forces generated by the exciter AMBs are compared to the gyroscopic forces the rotor would experience which are calculated based on 30% of original gyroscopic matrix G. For this comparison, we first observe that the gyroscopic matrix G results from Disk

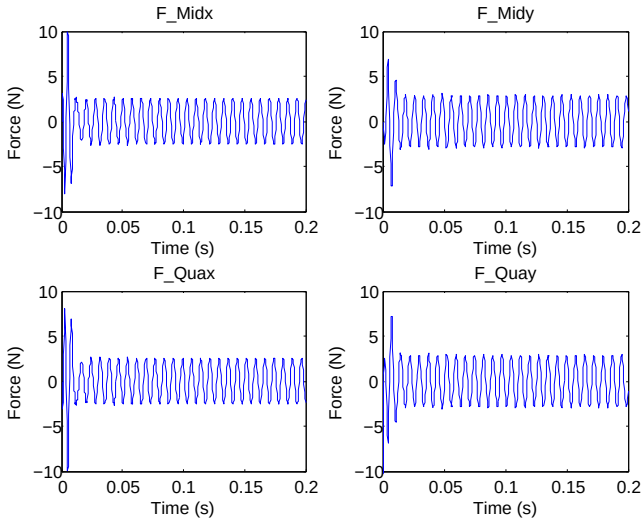

Figure 7: Emulated gyroscopic forces generated by the exciter AMBs.

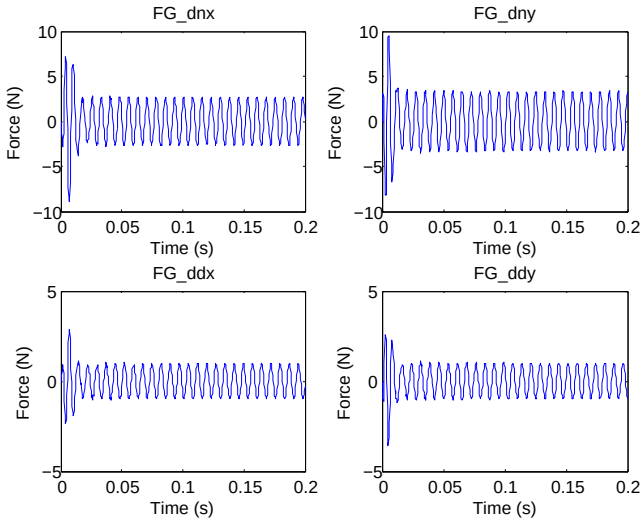

Figure 8: Actual forces caused by the gyroscopic matrix G at the support AMBs.

1 on the rotor AMB test rig. Therefore, in order to present a relevant comparison between the gyroscopic effects of similar rotors, with gyroscopic forces represented at opposite sides of the flywheel disk, the forces due to the matrix G are also shown at the locations of the support AMBs. With this observation, the gyroscopic forces in both cases are on opposite sides of the main disk to reveal a similar pattern between the emulated gyroscopic forces and the actual forces caused by the gyroscopic matrix G.

Shown in Fig. 7 is the emulated gyroscopic forces generated by the exciter AMBs at the speed of 8,000 rpm. Figure 8 shows the actual forces caused by the gyroscopic matrix G at the locations of the support AMBs. It can be observed that the pattern of the emulated gyroscopic forces and the actual gyroscopic forces are similar. There is a difference in the magnitude of the forces due to the difference in the size and location of the contributing disks, but the relative phase and frequency of the gyroscopic forces are well aligned, which demonstrates that the proposed emulation approach is feasible.

C. Experimental Results

The proposed emulation approach is also experimentally validated on the AMB test rig described in Section II. Since the generator negative stiffness causes negligible effect on rotor dynamics, here only the gyroscopic effect of the flywheel disk is emulated on the test rig. Magnetic bearings D and G generate the required excitation forces in opposite directions and the rotor displacements are saved at 8,000 rpm. Shown in Figs. 9 and 10 are the sensor measurements of the rotor displacement at the support and exciter AMB locations, respectively. The exciter AMBs are switched on at around 33.1 s, and it is observed that the magnitude of the rotor displacement changes in both the x and the y axes. Specifically, the rotor displacements in the x-axis at the MID location and in the y-axis at the NDE location decrease, and increase at the remaining locations. Figs. 11 and 12 compare the rotor orbits without and with

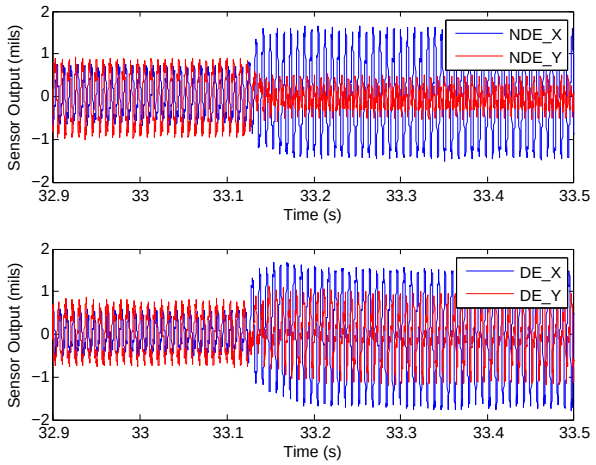

Figure 9: Sensor measurements at the support AMB locations.

the excitation forces. The figure comparisons reveal the tilting of the rotor, indicating that the rotor experienced precessions about the x and the y axes.

V. Conclusions

In this paper, an existing rotor-AMB test rig with exciter AMBs is adopted to emulate the operation of energy storage flywheels. The two AMBs at the mid and quarter spans of the shaft are used to emulate the negative stiffness of the generator and the gyroscopic effect of the flywheel disk. The simulation results have shown the negative stiffness provided by the generator causes a negligible effect on the rotor dynamics. The emulated gyroscopic forces generated by the exciter AMBs are similar to the actual gyroscopic forces produced by the gyroscopic matrix obtained from a previous finite element analysis, which demonstrates that the emulation approach presented in the paper is feasible.

For the future work, we will design a controller to improve the stability and performance of the rotor-AMB test rig in the

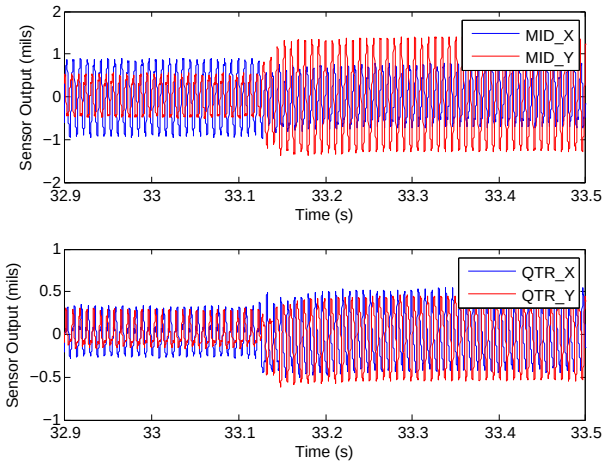

Figure 10: Sensor measurements at the exciter AMB locations.

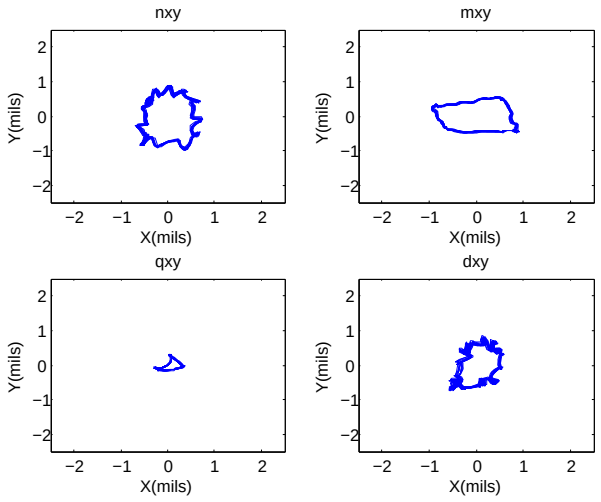

Figure 11: Rotor orbits without excitation forces.

presence of the emulated gyroscopic forces of the flywheel disk.

VI. Acknowledgements

This work was supported in part by the Key Project of Hubei Provincial Natural Science Foundation (No. 2009CDA028) and the China Scholarship Council.

References

[1] P. F. Ribeiro, B. K. Johnson, M. L. Crow, A. Arsoy and Y. Liu, "Energy storage systems for advanced power applications," *Proceedings of the IEEE*, vol. 89, no.12, pp.1744-1756, 2001.

[2] C. M. Reid, T. B. Miller, M. A. Hoberecht, P. L. Loyselle, L. M. Taylor, S. C. Farmer and R. H. Jansen, "History of electrochemical and energy storage technology development at NASA Glenn Research Center," *Journal of Aerospace Engineering*, vol. 26, no. 2, pp. 361-371, 2013.

[3] R. Hebner, J. Beno, and A. Walls, "Flywheel batteries come around again," *IEEE Spectrum*, vol. 39, no. 4, pp. 46-51, 2002.

[4] S.M. Lukic, J. Cao, R.C. Bansal, F. Rodriguez and A. Emadi, "Energy storage systems for automotive applications," *IEEE Transactions on Industrial Electronics*, vol. 55, no. 6, pp. 2258-2267, 2008.

[5] J. G. Bitterly, "Flywheel technology: Past, present and 21st century projections," *IEEE aerospace and electronic systems magazine*, vol. 13, no. 8, pp. 13-16, 1998.

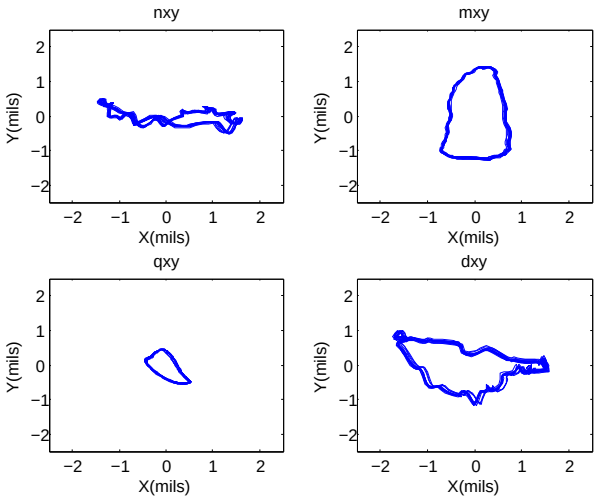

Figure 12: Rotor orbits with excitation forces.

[6] G. O. Cimuca, C. Saudemont, B. Robyns and M. M. Radulescu, "Control and performance evaluation of a flywheel energy-storage system associated to a variable-speed wind generator," *IEEE Transaction on Industrial Electronics*, vol. 53, no. 4, pp. 1074-1085, 2006.

[7] G. V. Brown, A. Kascak, R. H. Jansen, T. P. Dever and K. P. Duffy, "Stabilizing gyroscopic modes in magnetic-bearing-supported flywheels by using cross-axis proportional gains," in *Proceedings of the AIAA Guidance, Navigation, and Control Conference*, San Francisco, California, 2005, pp. AIAA-2005-5955.

[8] T. P. Dever, G. V. Brown, K. P. Duffy and R. H. Jansen, "Modeling and development of a magnetic bearing controller for a high speed flywheel system," in *Proceedings of the 2nd International Energy Conversion Engineering Conference*, Providence, RI, 2004, pp. AIAA-2004-5626.

[9] M. Ahrens and L. Kucera, "Cross feedback control of a magnetiic bearing system," in *Proceedings of 3rd International Symposium on Magnetic Suspension Technology*, Tallahassee, Florida, 1995, pp. 177-191.

[10] M. Ahrens, L. Kucera and R. Laesonneur, "Performance of a magnetically suspended flywheel energy storage device," *IEEE Transactions on Control Systems Technology*, vol. 4, no. 5, pp. 494-502, 1996.

[11] L. A. Hawkins, B. T. Murphy and J. Kajs, "Analysis andtesting of a magnetic bearing energy storage flywheel with gain-scheduled, MIMO control," in *Proceedings of ASME Turboexpo*, Munich, Germany, 2000, pp. 1-8.

[12] S. Sivrioglu, K. Nonami and M. Saigo, "Low power consumption nonlinear control with H_∞ compensator for a zero-bias flywheel AMB system," *Journal of Vibration and Control*, vol. 10, pp. 1151-1166, 2004.

[13] S. Sakai, K. Kuriyama and K. Nonami, "A novel passivity based control of active magnetic bearing systems without conventional cross feedback," *Journal of System Design and Dynamics*, vol. 3, no. 4, pp. 540-550, 2009.

[14] S. E. Mushi, "Robust Control of Rotordynamic Instability in Rotating Machinery Supported by Active Magnetic Bearings," Ph.D. Dissertation, Uniersity of Virginia, Charlottesville, VA, 2012.

[15] L. Di and Z. Lin, "Control of a flexible rotor active magnetic bearing test rig: a characteristic model based all-coefficient adaptive control approach," *Control Theory and Technology*, vol. 12, no. 1, pp. 1-12, 2013.

[16] P. E. Kascak, T. P. Dever and R. H. Jansen, "Magnetic circuit model of PM motor-generator to predict radial forces," in *Proceedings of 1st International Energy Conversion Engineering Conference*, Cleveland, 2003.

[17] S. Y. Yoon, Z. Lin, T. Dimond and P. e. Allaire, "Control of active magnetic bearing systems on non-static foundations," in *Proceedings of the 9th IEEE International Conference on Control and Automation (ICCA)*, Santiago, Chile, 2011, pp. 556-561.

[18] M. I. Friswell, J. E. T. Penny, S. D. Garvey and A. W. Lees, " *Dynamics of Rotating Machines*. Cambridge: Cambridge University Press, 2010.